Water Resources Research

RESEARCH ARTICLE
10.1029/2018WR024434

# Computational Modeling of Fine Sediment Relocation Within a Dam Reservoir by Means of Artificial Flood Generation in a Reservoir Cascade

**E. Bladé Castellet[1], M. Sánchez-Juny[1], M. Arbat Bofill[1], and J. Dolz Ripollés[1]**

[1]Flumen Institute (UPC-CIMNE), Barcelona, Spain

**Key Points:**
- The relocation processes of fine sediment in a reservoir are measured and analyzes
- A numerical model for prediction of reservoir sediment dynamics is calibrated
- Different management strategies to enhance sediment-relocation processes are analyzed

**Correspondence to:**
E. Bladé Castellet,
ernest.blade@upc.edu

**Citation:**
Bladé Castellet, E., Sánchez-Juny, M., Arbat Bofill, M., & Dolz Ripollés, J. (2019). Computational modeling of fine sediment relocation within a dam reservoir by means of artificial flood generation in a reservoir cascade. *Water Resources Research*, *55*. https://doi.org/10.1029/2018WR024434

Received 17 NOV 2018
Accepted 24 MAR 2019
Accepted article online 2 APR 2019



**Abstract** Sediment relocation is a process where water turbulence moves deposits from shallower to deeper zones of a lake or reservoir. Additionally, in the context of a reservoir cascade relocation is a one of the possible sediment management strategies used to maintain the operational capacity of reservoirs. Numerical modeling tools applied to sediment dynamics can help to better understand the reservoir sedimentary processes and enhance the design of management strategies. This paper describes the detailed analysis of the cohesive sediment dynamics within a reservoir and a methodology for the calibration of numerical models for the management of sediment deposits through dam operation and upstream generation of artificial floods. The calibration process was based on an accumulated sediment volume curve and the usage of simplified models for an initial parameter estimation. The calibrated model has been applied to analyze different possibilities of sediment relocation strategies.

**Plain Language Summary** This paper describes the detailed analysis of the sediment dynamics of a reservoir and how the analysis can be used for model calibration. Furthermore, it presents a methodology to build and calibrate a two-dimensional (2-D) model for reservoir sediment dynamics and a case study of cohesive fine sediment management in a reservoir. Sediment relocation consists of the resuspension of sediments in shallower zones by waves and water currents with subsequent transport to and settling in deeper zones. In this work, we suggest a simple procedure to graphically represent the relocation processes. The proposed calibration process is based on the usage of simplified models for an initial parameter estimation. The method has been exemplified with a real case in the Riba-roja reservoir in the Ebro River (Iberian Peninsula).

## 1. Introduction

Sediment transport and deposition are common, unavoidable processes in reservoirs; one of their main impacts is storage loss (Mahmood, 2005; Wen Shen, 1999). Storage loss may impair the reservoir finality, including water supply, hydropower, flood control, and recreational uses. Additionally, there are impacts of reservoir sediment retention on water quality, such as the reduction of sediment load downstream and an increase of water turbidity and oxygen demand (Prats Rodríguez et al., 2014). Moreover, the accumulation of deposits in deltaic form in the reservoir tail can produce several adverse effects, including upstream flooding, impaired navigation, and impingement on wildlife and their habitat (Kostic & Parker, 2003).

Sediment relocation in reservoirs and lakes can take place naturally or in an induced manner. Likens and Davis (1975) described the resuspension of sediments in shallower zones by waves and water currents with subsequent transport to and settling in deeper zones. They used the term *sediment focusing* to refer to these processes. Blais and Kalff (1995) also used that term, describing the different possible patterns of sediment focusing or relocation and emphasizing the importance of the same, for a variety of studies to assess the area occupied by the zones of erosion, transportation, and accumulation.

To maintain the operational capacity of reservoirs and limit the aforementioned problems, several sediment control strategies are used (Morris et al., 2008), these include sediment yield reduction, sediment storage, sediment routing, sediment removal, and sediment focusing or relocation. The most obvious of these, which has proven to be a good alternative in many cases (Palau Ybars, 1998; Wang & Hu, 2009), would be sediment release. However, in long reservoirs, where the sediments are mainly deposited in the tail, this might be impossible or extremely expensive. Sediment relocation encompasses hydraulic techniques to tactically

rearrange sediments within the impoundment to solve localized problems; numerical modeling can be a useful tool to design and evaluate different relocation alternatives. (Felix et al., 2016; James & Barko, 1993). Numerical models capable of simulating suspended sediment transport in aquatic environments are valuable and increasingly used tools for the better understanding and prediction of reservoir sediment dynamics (Castillo et al., 2015; Gibson & Boyd, 2014; Guertault et al., 2016; Tarekegn et al., 2014). The tool used for this study is the freeware package Iber (www.iberaula.com; Bladé, Cea, Corestein, Escolano, et al., 2014), which is based on the solution of the 2-D shallow water equations using the finite volume method (Vázquez-Cendón, 1999). The Iber software includes sediment (suspended and bedload) transport modules.

The final aim was to use numerical simulation to design sediment management strategies for the Ribaroja reservoir.

To achieve this goal, the partial objectives are as follows:

1. The analysis of the reservoir bed changes during a flood episode where sediment relocation was observed.
2. The calibration of a 2-D sediment dynamics numerical model with the data of the sedimentary processes related to the flood episode.
3. The assessment of the performance of fine sediment relocation strategies within a reservoir in a reservoir cascade.

## 2. Methods

### 2.1. Numerical Model

As indicated in the introduction, the tool used for the present study is the Iber software package, which is a tool for numerical simulation of water flow and fluvial processes in rivers and estuaries (Bladé, Cea, & Corestein, 2014). Apart from solving the water hydrodynamics, Iber has a series of modules to solve different processes, such as bedload and suspended sediment dynamics, water quality, and hydrological processes. The numerical solver of the sediment transport is coupled to the hydrodynamic module, which solves the 2-D shallow water equations written using the finite volume method and the numerical scheme of Roe (Roe, 1986).

The reader is referred to Bladé, Cea, & Corestein, Escolano, et al. (2014) and the references therein for a detailed description and experimental validation of the numerical schemes used to solve the shallow water equations, which are not included in this paper for brevity. This hydraulic module has been applied to several studies in the past, including the river inundation modeling, overland flow (Cea & Bladé, 2015), evaluation of gully restoration measures (C. Castillo et al., 2014), wood transport in rivers (Ruiz-Villanueva et al., 2014), and water quality loss (Cea et al., 2016).

The sediment transport module includes bedload and suspended sediment transport; it is based on the results of velocity, depth, and turbulent viscosity fields computed by the hydrodynamic and turbulence modules. In this work, no bedload has been considered. The suspended sediment transport was modeled by solving the depth averaged turbulent convection-diffusion equation (1), using the method described in Cea et al. (2016).

$$\frac{\partial hC}{\partial t}+\frac{\partial hU_xC}{\partial x}+\frac{\partial hU_yC}{\partial y}=\frac{\partial}{\partial x_j}\left(\left(\Gamma+\frac{\nu_t}{S_{c,t}}\right)h\frac{\partial C}{\partial x_j}\right)+(E-D) \tag{1}$$

Here C is the depth-averaged concentration of suspended solids; $U_x$ and $U_y$ are the horizontal depth-averaged velocity components; $\nu_t$ is the turbulent viscosity; $\Gamma$ is the molecular diffusion coefficient for suspended solids; $S_{c,t}$, is the Schmidt number, which relates the moment turbulent diffusion coefficient with the suspended turbulent diffusion coefficient; $D$ is the deposition rate; and $E$ is the entrainment rate.

Under the assumption of no bedload, the variation of the bed level $Z_b$ is calculated with the sediment conservation equation:

$$(1-p)\frac{\partial Z_b}{\partial t}=D-E \tag{2}$$

$E$ was evaluated with the linear threshold model first proposed by Partheniades (1965) and Ariathurai and Arulanandan (1978) for cohesive soils.

$$E = M \cdot \left( \frac{\tau_b}{\tau_{ce}} - 1 \right) \quad (3)$$

Here the erosion rate depends on the difference between the shear stress $\tau_b$ and the strength (or erosion critical stress) $\tau_{ce}$, and on a parameter $M$ representative of the erosion rate ($M$ is the value of the erosion rate when $\tau_b = 2 \cdot \tau_{ce}$):

For $D$, the following widely used expression (Einstein & Krone, 1962), which considers a deposition critical stress, $\tau_{cd}$, was used:

$$D = \left( 1 - \frac{\tau_b}{\tau_{cd}} \right) \cdot W_s \cdot C_a \quad (4)$$

$C_a$ is a the near-bed concentration derived from the Rouse profile, calculated according to Huybrechts and Villaret (2010). $W_s$ is the settling velocity calculated using the Van Rijn formula (Van Rijn, 1987), which is commonly accepted in large scale applications (Duan & Nanda, 2006).

To create and calibrate the numerical model, the geometry data, initial conditions, and boundary conditions are required. The geometric data were obtained through bathymetric campaigns. The initial and boundary conditions were the discharges and water levels provided by the water administration and dam operation companies (Section 3.2).

### 2.2. Calibration Process

The calibration process consisted of the following steps:

1. Description of the reservoir bottom evolution. To describe this evolution, an accumulated sediment volume (ASV) curve was used (see section 4.1). This curve was obtained from the data of two bathymetries on different dates, before and after a flood.
2. Construction of a simplified numerical model, which uses a large element size mesh to minimize the computational time.
3. First estimation of parameters using the simplified model and the Monte Carlo method, which requires a large number of simulations.
4. Construction of a detailed numerical modeling using a fine element mesh.
5. Operation of the detailed numerical modeling for a final manual adjustment of parameters to fit the numerical results with the observed ASV curve (step 1). The manual adjustment is based on the information of the effect of the parameters on the computed ASV curve from step 3.

No further validation tasks have been planned presently. Such work would require the agreement of all the actors and stakeholders involved in the reservoir management and exploitation (including water administration, municipalities, energy companies, irrigation user community, and environmental nongovernmental organizations), which is not envisaged in the short term.

## 3. Case Study

### 3.1. Study Area

The Ebro River basin has an area of about 85,000 km$^2$, covering a major part of the northeast Iberian Peninsula. The basin has more than 107 reservoirs of more than 1-hm$^3$ capacity; the irrigated area has an extension of about 800,000 ha. The Riba-roja reservoir is located immediately downstream of the Mequinensa reservoir (Figure 1), the largest reservoir of the Ebro River. Both reservoirs are situated in the lower Ebro River. The distance between the Riba-roja Dam and the river mouth is 115 km.

Riba-roja is a monomictic long and narrow reservoir, with a fairly regular morphology. The present storage capacity is of 210 hm$^3$ and its residence time is of a few weeks. A gravity dam with its crest at an elevation of 76 m above the sea and the base at 16 m closes the Riba-roja reservoir downstream. Added to the main Ebro River flow, this receives important discharge input from two tributaries—the Segre and Cinca Rivers, which drain from the central Pyrenees and converge approximately 2 km before the confluence with the Ebro River at the tail of the reservoir. The present work focuses on the shallow areas at the tail of the reservoir, where the hydrodynamic conditions are similar to those of river flow (Arbat Bofill, 2015).

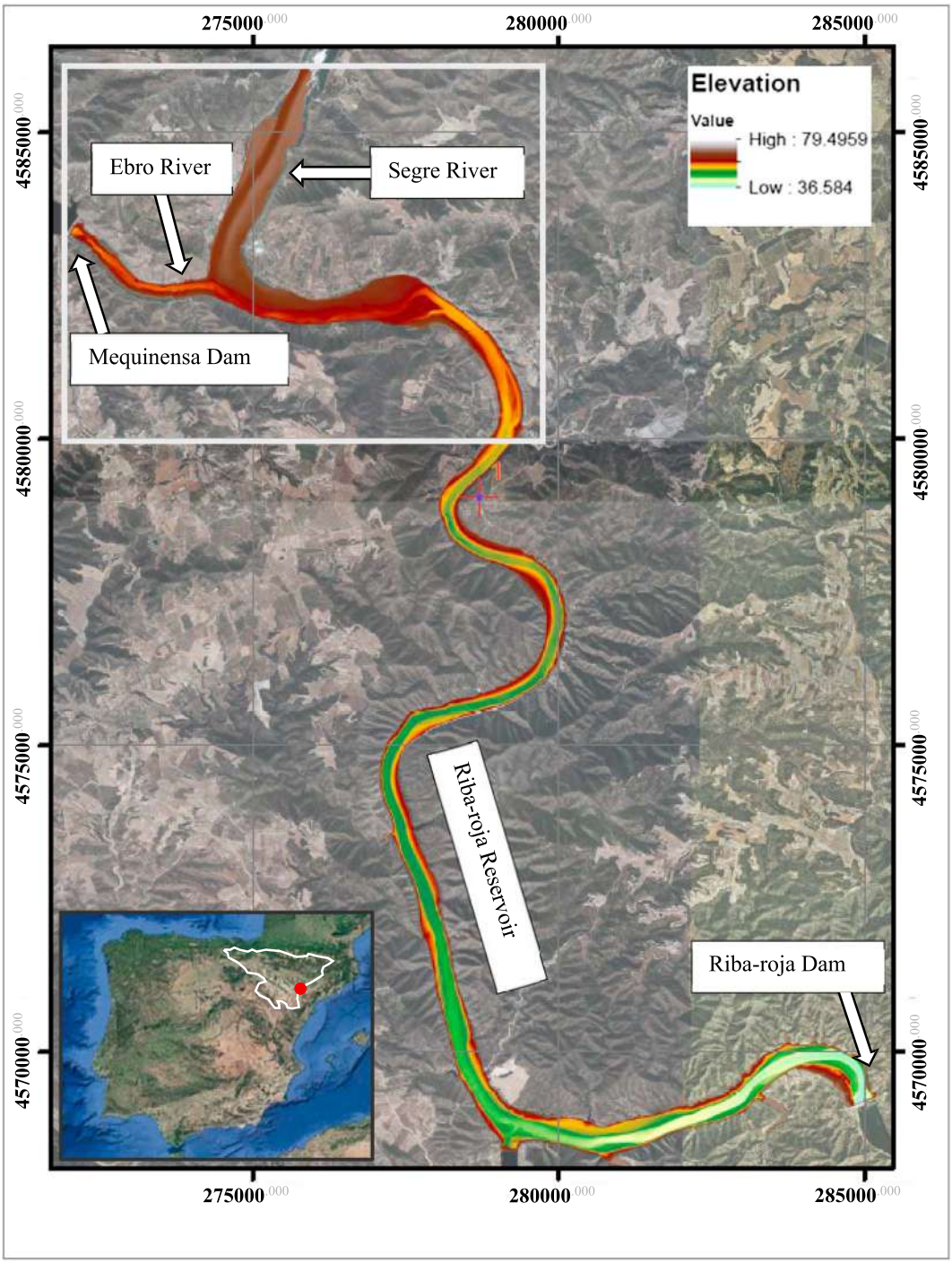


**Figure 1.** Riba-roja reservoir location and 2007 multibeam bathymetry shown as a 2 × 2-m raster (color scale) covering the whole reservoir. Study area highlighted with the white rectangular frame (source of background image: Google Earth.). In the corner map, the red point indicates the reservoir location and the white line indicates the watershed extension.

In recent years, the natural sediment yield of the Segre River has significantly increased due to the sediment release between 1995 and 1997 through the bottom outlets of the Barasona Dam on Essera River, one of its tributaries. Since its construction, the Barasona reservoir has experienced acute siltation problems at a rate between 0.3 and 0.5 $hm^3$ of deposited sediment annually (Lobera et al., 2016). The successful sediment release operations resulted in more than 9 $hm^3$ of sediment accumulated during decades in the reservoir

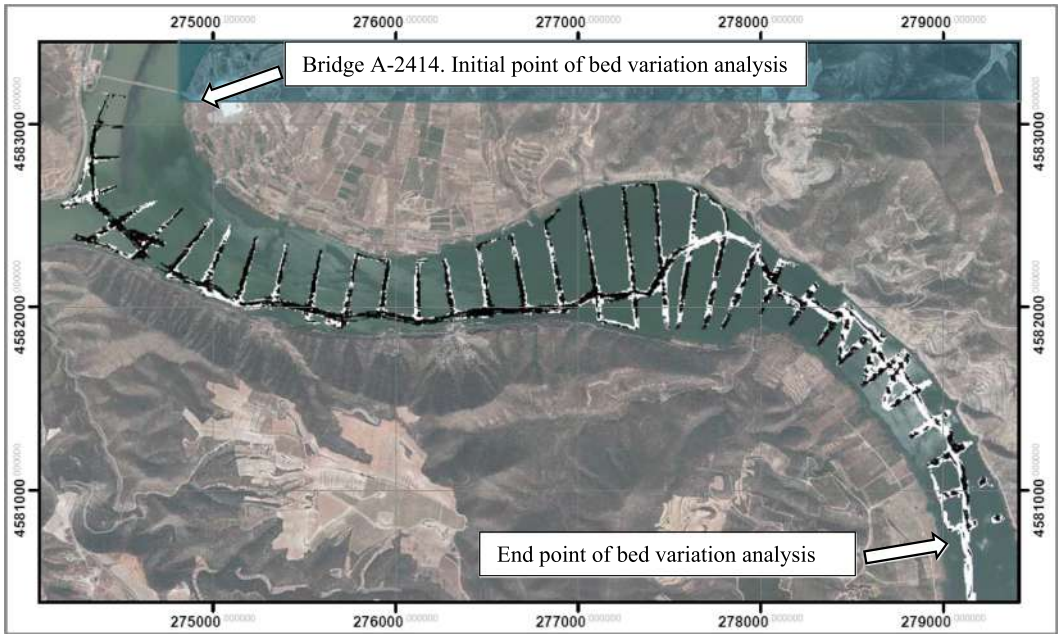


**Figure 2.** Area, within the study area shown in Figure 1, covered by the 2008 bathymetry, showing the path of the single beam sensor along the thalweg and cross sections from the Ebro and Segre Rivers confluence (top left) downstream (bottom right). Areas of erosion are shown in black, while areas of deposition are shown in white.

base sluiced downstream (Avendaño et al., 2000; Palau Ybars, 1998). This sediment is presently reaching the tail of the Riba-roja reservoir (the current study area).

At the tail of Riba-roja reservoir, the Ebro River has an average annual contribution of 8,009 $hm^3$ (Dolz et al., 2009). The flow of the tributary Segre increases the contribution to 14,069 $hm^3$ downstream of the Riba-roja (Dolz et al., 2009). In percentages, the Ebro River transports 58.82% of the total discharge into the Riba-roja reservoir, while the Segre River carries the rest (Dolz et al., 2009).

Throughout almost the totality of the reservoir extension, the sediments have a silt-clay texture, with a silt ($4\ \mu m < \phi < 63\ \mu m$) percentage between 56% and 74% and a clay ($\phi < 4\ \mu m$) percentage between 18% and 43% depending on the area (López et al., 2012; Roura Carol et al., 2008).

### 3.2. Acquisition of Field Data

With the aim of studying the bottom evolution and the sediment dynamics in the Riba-roja reservoir tail, in autumn 2007, a bathymetric campaign was performed, covering the whole area of the reservoir. Thereafter, significant floods took place in May–June 2008. After the floods, to evaluate the morphologic changes in the reservoir bottom, a new bathymetry was executed in December 2008. It is worth noting that no other significant flood took place between the two bathymetries.

For the field bathymetric campaign of autumn 2007, a multibeam sensor was used. This technique provided a continuous bathymetry, in contrast to the simple beam technique. The final product was a digital terrain model in raster format with a $2 \times 2$ m cell size (Figure 1). In December 2008, the second bathymetric campaign was performed, focusing only on the area of interest (the tail of the reservoir). Here due to the available resources, a simple beam sensor was used; the data were only gathered along a path following the thalweg of the river and several perpendicular cross sections, one approximately every 200 m (Figure 2). Moreover, the results were converted to a raster format but now only contained data along a series of transversal strips and a longitudinal profile of the width covered by the sensor.

In the period between the October/November 2007 and December 2008 bathymetries, there was only one major flood episode, lasting from late May to early June 2008. The flood came into the Riba-roja reservoir from the Segre River and the Mequinensa Dam (Ebro River). The peaks of the Segre River hydrograph took place 5 days before the peak of the Ebro River (Mequinensa Dam), as is shown in Figure 3.

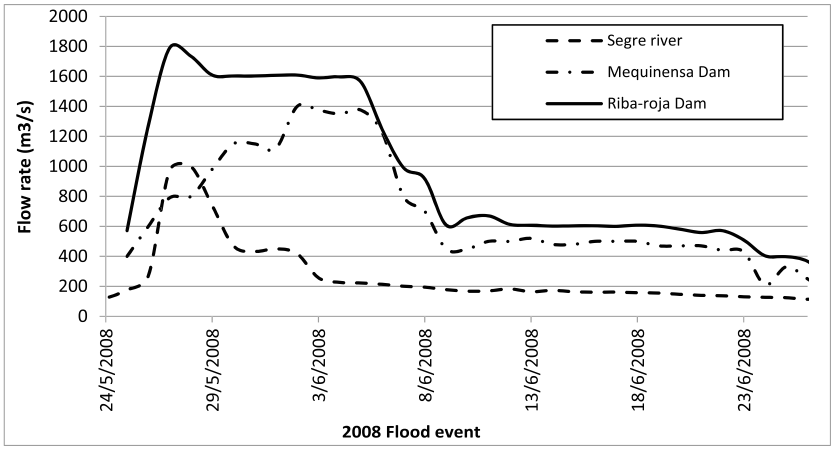


**Figure 3.** Average daily flows, used as boundary conditions in the calibration of the numerical model, at Segre River (inflow), Mequinensa Dam (inflow), and Riba-roja Dam (outflow), for the period corresponding to the May–June 2008 flood.

In the Segre River, the peak discharge was 1,000 $m^3$/s; it soon decreased below 400 $m^3$/s and finally to less than 200 $m^3$/s. The discharge released through the Mequinensa Dam had a peak of major 1,400 $m^3$/s. The addition of these two flows is the hydrograph entering the Riba-roja reservoir, with an initial peak of 1,800 $m^3$/s and a consequent recession to a flow around 1,600 $m^3$/s. During an 11-day period, the mean discharge into the Riba-roja reservoir was greater than 1,400 $m^3$/s (the mean average inflow is around 260 $m^3$/s). During the flood, Riba-roja Dam was operated to maintain constant water levels at normal elevation (69.5 m) for hydropower generation purposes. As the water elevation was nearly constant and the volume of the reservoir not too large, the outflow from the reservoir was similar to the inflow (Segre and Ebro Rivers). These inlet and outlet flow hydrographs were the boundary conditions used during the calibration of the numerical model.

## 4. Results

### 4.1. Sediment Dynamics

A first analysis of the reservoir bed evolution between autumn 2007 and December 2008 was performed by comparing the two digital terrain models. Since both bathymetries were in raster format, performing the difference of the bathymetries was straightforward. The result of the raster subtraction is shown qualitatively in Figure 2. It shows that the upstream reach has a clear erosive trend (black), while there is mainly deposition downstream. Apart from this qualitative analysis, the raster substation allowed was the base for a quantitative analysis with the aim of representing and quantifying the spatial distribution of the sediment. The overlapping area of the two bathymetries was divided into subareas, each subarea covering the whole reservoir width and a longitudinal distance, or segment, 200 m in length, which is the distance between cross sections of the bathymetry path. For each subarea, the average deposition (+) or erosion (−) height was calculated. Thus, the longitudinal average deposition/sedimentation profile shown in the dashed line of Figure 4 was obtained. Here it can be seen that in the first 4,000 m, the erosion processes predominate, while there is primarily deposition downstream.

An alternative way to represent the erosion/deposition patterns along the reservoir is the ASV curve. To obtain this curve, the total deposited (+) or eroded (−) volume for each of the aforementioned subareas was calculated by multiplying the surface of each area by the average bottom variation and then added to the deposited volume of all upstream areas. This process led to the curve of accumulated deposited or eroded volume shown in continuous line in Figure 4. The curve showing the volume eroded in the first upstream 4,000 m of the reservoir tail is fairly similar to the volume of sediment settled in the next 4,000 m downstream. Thus, in this area, a sediment volume of about 170,000 $m^3$ was displaced approximately 4 km downstream in the period between the two bathymetries. As the ASV curve is the result of averaging in the width

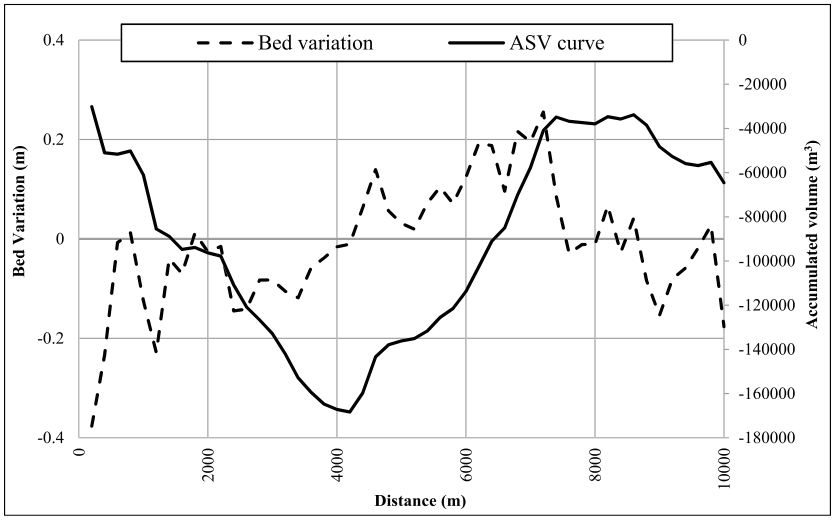


**Figure 4.** Width averaged bed variation (negative values mean erosion and positive values indicate deposition) in the May–June 2008 flood and the ASV curve along the reach covered by the 2008 bathymetry (shown in Figure 2). Origin of distances is at the A-2414 road bridge.

and integrating along the reservoir axis, it represents the global erosion and deposition patterns, thus filtering the oscillations inherent to the bathymetries precision in a punctual analysis.

### 4.2. Calibration Process

For the calibration process, the May–June 2008 flood was simulated. The idea was to perform a first parameter estimation working with a simplified set of models and then fine tune the calibration with more complex models. A very simple model was used in the beginning, which was successively refined until reasonable fitting with the experimental data was achieved. For the current case, this process required only one iteration (a first model with one element in the width and a second model with three elements in the width). Thereafter, the parameters from these simplified models acted as input data for a much more detailed model (fine mesh) and were manually adjusted until the best fitting with the experimental data was obtained (Figure 5).

The numerical model based on the equations has been presented in section 2.1. The calibration process consisted of obtaining a set of values for parameters $M$, $\tau_{ce}$, and $\tau_{cd}$ and the sediment diameter $d$ (which affects the settling velocity $W_s$) to analyze the fitting of the computed ASV curve to that resulting from the experimental data (Figure 4). The criteria for selecting the best set of parameters was the value of the minimum quadratic error. For this purpose, a basic probabilistic Monte Carlo method was used with repeated random sampling of the previous parameters. As no data of grain size distribution were available, the calibration focused on the description of the previous parameters without entering into more detail as for example grain sorting analysis.

In the numerical model, the water flow boundary conditions were the hydrographs shown in Figure 3. The initial condition was a constant water elevation in the whole reservoir, equal to 69.5 m. The sediment boundary condition at the Segre River was the equilibrium solid discharge concentration. At the Ebro River, the boundary condition was clear water due to the presence of the Mequinensa Dam immediately upstream.

As a great number of scenarios had to be simulated, as is outlined before, at the first stage, a very simple mesh was to be used to minimize the number of computational elements. This first mesh consisted of only one element in the width of the channel, one element corresponding to each cross section of the 2008 bathymetry (Figure 6a), and similar elements for the rest of the reservoir.

With the first mesh, after a series of preliminary simulations to adjust the range of variation of the parameters, 10,000 simulations were performed randomly sampling the values of $M$ between 0 and $5 \cdot 10^{-7}$ m/s, $\tau_{ce}$ between 0 and 3 Pa, and $\tau_{cd}$ between 0 and 2 Pa. As for the diameter, data has been based on Dolz et al.'s (2009) study. Here the sediment samples were obtained at 16 points within the reservoir, 7 of them in the

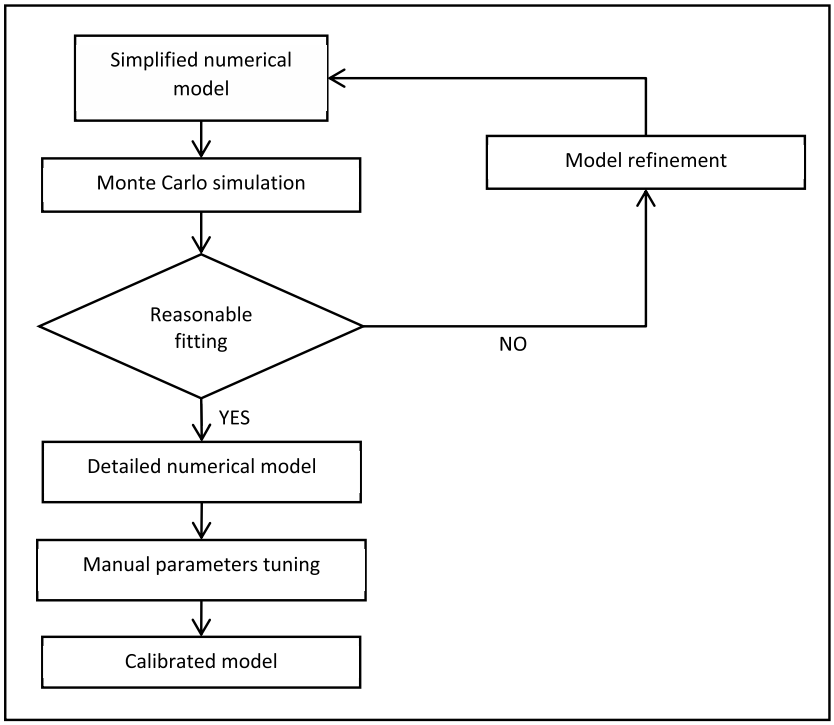


**Figure 5.** Flowchart of the calibration process proposed in the present study.

current study area. The results of the samples indicated a mean sediment diameter between 7 and 107 μm, with high variability (standard deviations greater than the mean), and a high correlation between kurtosis and asymmetry. Owing to this, the diameter was not fixed but allowed to vary in a range of 10 to 100 μm. It should to be taken into account that the numerical model used a uniform diameter hypothesis; thus, the value of the diameter had be the one that better represented the observed sediment dynamics and not an average of the sample diameters.

After the first set of simulations, a poor agreement between the numerically obtained ASV curve and the experimental one was observed. The criteria to decide the goodness of fit between the numerical and experimental curves was the sum of squares of the differences between the experimental and the numerical ASV curve at each mesh element. The six curves with better fitting, named S1 to S6, are shown in Figure 7a. Part of the differences can be attributed to the simplicity of the mesh being used. From the field data, it was observed that there is a transversal variability of the erosion and deposition process due to the transversal variation of velocity, depth, and, consequently, shear stress. This effect cannot be reproduced with only one computational element in the whole width. Thus, in the second stage, the computational mesh was refined considering three elements in the width of the reservoir and adjusting the mesh of the elements to

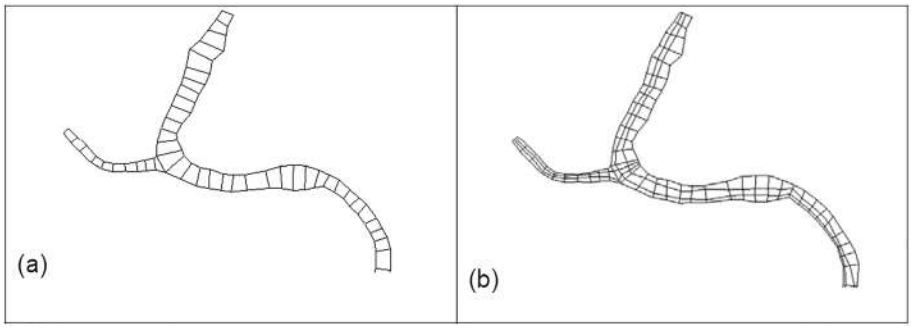


**Figure 6.** Initial mesh with (a) one element in the width and (b) mesh with three elements in the width.

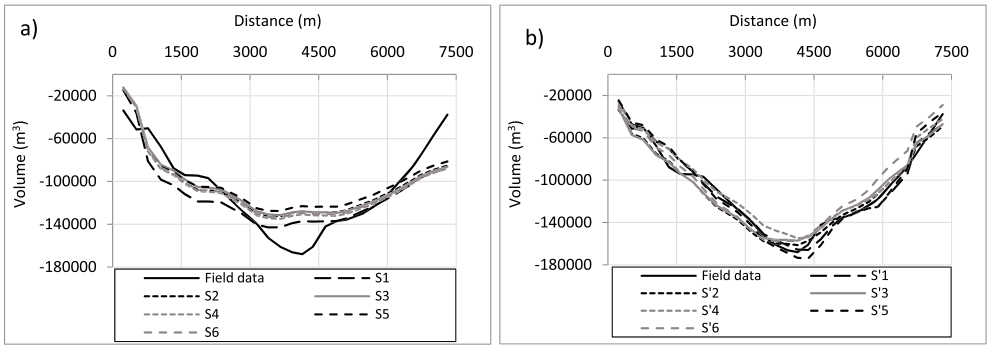


**Figure 7.** Comparison of the experimental accumulated sediment volume curve (field data) with the simulated curve obtained with the initial mesh (a) and the mesh with three elements in the width (b).

preserve the continuity of the main channel along the model as much as possible, as is shown in Figure 6b. In Figure 7b, the six curves with better fit using this mesh, named S′1 to S′6, are shown. Here much better fitting was achieved as the curves represented the descendant and rising branches more accurately, in addition to the minimum point.

Table 1 shows the values of the parameters $M$, $\tau_{ce}$, and $\tau_{cd}$ and the sediment diameter $d$ that minimizes the sum of squared differences between the experimental and accumulated volumes. It can be observed that for S′1, S′4, and S′5, the shear strength is lower than the deposition shear stress ($\tau_{ce} < \tau_{cd}$), while for S′2 and S′3, the opposite is true ($\tau_{ce} > \tau_{cd}$).

In spite of all six results showing good fitting with the experimental erosion/sedimentation data, according to the authors, cases with $\tau_{cd} < \tau_{ce}$ present a lesser degree of physical sense since it implies a range where neither deposition nor sedimentation is produced. Nevertheless, previous work exists, such as those by Antoine et al. (2014), who fitted their field data to values with $\tau_{cd} > \tau_{ce}$.

Finally, since one of the objectives was to develop a detailed 2-D model to work with different sediment management strategies, a model with a fine triangular mesh has been built. The model used an element size of 20 m and a total of 63,428 elements. Figure 8 shows details of the mesh corresponding to the junction area.

The detailed 2-D model was first launched (simulation S″0) with the best fitting parameters of the simplified model (simulation S′1). Due to the different detail of the mesh, resulting in a more detailed depth and velocity distribution, the results of this last set of simulations, with the 2-D detailed mesh and the parameters of S′1, did not fit too well with the field ASV curve (simulation S″0 of Figure 9). Thus, five more simulations with the detailed 2-D mesh were prepared, varying the parameters. Looking at the tendencies of the thousands of results of simulations S′, it was seen that to adjust the aforementioned curve S″0 to the field data, $M$, $d$, and $\tau_{cd}$ would have to be reduced, while $\tau_{ce}$ would have to increase. Using this reasoning, assuming the influence on the results of the variations of the parameters was not linear, the five simulations S″1 to S″5 in Table 2 were prepared. The architecture of Iber allowed all five models to be launched in parallel, saving time. Among the five results, S″2 had minimum quadratic error. Figure 9 shows the comparison between the experimental ASV curve and the ones obtained from these S″ simulations using the detailed triangular mesh model.

**Table 1**
*Parameters of the Six Best Fitting Simulations (Using the Minimum Quadratic Error Criteria) Obtained With Monte Carlo Method Using the Mesh With Three Elements in the Width*

| Parameter | S′1 | S′2 | S′3 | S′4 | S′5 | S′6 |
|---|---|---|---|---|---|---|
| $M$ (m/s) | **$8.1 \cdot 10^{-8}$** | $1.21 \cdot 10^{-7}$ | $1.30 \cdot 10^{-7}$ | $9.0 \cdot 10^{-8}$ | $7.2 \cdot 10^{-8}$ | $1.02 \cdot 10^{-7}$ |
| $\tau_{cd}$(N/m$^2$) | **1.235** | 1.454 | 1.533 | 1.363 | 1.104 | 1.246 |
| $\tau_{ce}$ (N/m$^2$) | **0.989** | 1.883 | 1.907 | 1.153 | 0.98 | 1.997 |
| $d$ (μm) | **40.25** | 25.47 | 25.20 | 35.56 | 42.96 | 27.04 |

*Note*. S′1 (in bold) corresponds to the set of parameters with better fitting.

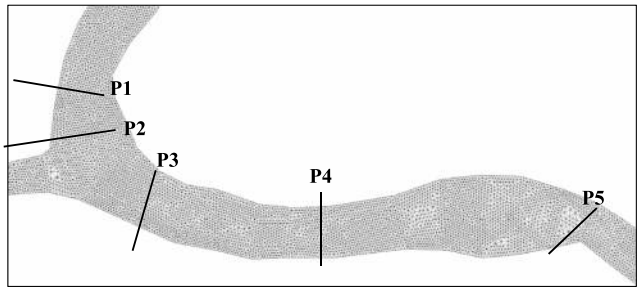


**Figure 8.** Position of the cross sections used for sediment volume evaluation shown on the fine mesh used in the final model.

### 4.3. Application

The previous sections presented the method used for calibration of the sediment transport numerical model of the Segre and Ebro Rivers' confluence, located at the tail of Riba-roja reservoir. This section presents an example case for using the numerical model to analyze the results of sediment management strategies. However, the paper does not strive to propose a specific, detailed sediment management strategy, recommendations, or guidelines. That corresponds to the reservoir managers.

The case consists of comparing two, different, possible reservoir operations during and after a hypothetical three-day long flood in the Segre River with a constant discharge of 600 $m^3/s$, followed by a normal discharge of 80 $m^3/s$. The two scenarios that have been analyzed are as follows:

A. Normal reservoir operation: Riba-roja reservoir water elevation is maintained at its normal level, at 69.5 m above sea level. The Mequinensa Dam is operated normally, releasing 600 $m^3/s$ (which is the hydropower plan nominal discharge) during 14 hr and with no discharge for the rest of the day (Figure 10a).
B. Sediment relocation strategy: Release of 840 $m^3/s$ through the Riba-roja Dam during the occurrence of the flood, to have a partial drawdown of approximately 6 m. In the Mequinensa Dam, the discharge is increased to 1,400 $m^3/s$ (600 $m^3/s$ through the turbines and 800 $m^3/s$ through the dam gates) during the same 14-hr period.

The objective of Scenario B was to facilitate sediment entrainment by increasing the bed shear stress as the velocity of the flow increased; this was owed to two reasons: the higher discharge as compared to Scenario A and the partial drawdown.

To check the differences in sediment transport between the two scenarios, the water discharge, sediment discharge, and solid volume crossing the five characteristic cross sections of Figure 8 were evaluated, as is shown in Figures 11 to 14. The first cross section (Section P1) was located in the bridge over the Segre River, just upstream from the confluence with the Ebro River. The second cross section (Section P2) was immediately upstream of the confluence. The third cross section was downstream of the junction. The fourth cross section (Section P4) was located in a narrow point of the Riba-roja reservoir, approximately 2,150 m downstream of section 1, measuring the distance along the reservoir axis. The last cross section (Section P5) was downstream of a wide area, after a curve to the right, and approximately 2,400 m of the previous one.

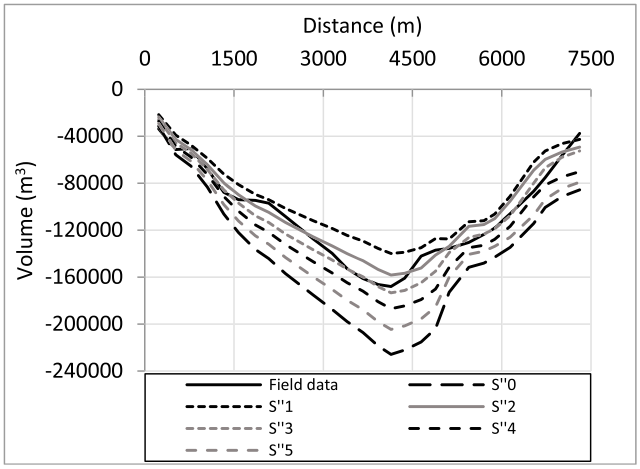


**Figure 9.** Comparison of the experimental accumulated sediment volume curve (field data) with the curves obtained by numerical simulations in Table 2 in the last triangular fine mesh model.

The calculated flow hydrographs at P2 and P3 cross sections, immediately upstream and downstream of the confluence, are presented in Figure 11. The discharges are quite similar to the upstream boundary conditions shown in Figure 10, but with the effect of waves generated during the turbines starting up and shutting down and the opening and closing of the gates. Discharges in P1 (not shown) are almost identical than the discharges in P2, while discharges in P4 and P5 (not shown) are almost identical than those in P3. Figure 12 shows the evolution of the water surface. In Scenario A, the water elevation was maintained constant at the initial 69.5 m, the normal elevation of the reservoir. In Scenario B, a significant 6-m decrease in water elevation was induced to obtain higher velocities facilitating sediment transport from the reservoir tail to the deepest areas of the reservoir.

Figure 13 shows the solid discharge for the two scenarios. For the first 3 days of constant flood and no release from the Mequinensa Dam, the effect of lowering the reservoir water level in Scenario B had a significant effect on solid discharges. For these 3 days, the water discharges for the two scenarios were exactly the same; it can be seen that in Section P1 the sediment discharge in Scenario B is more than twice the sediment

**Table 2**
*Parameters Used in Simulations Using the 2-D Fine Mesh Model*

| Parameter | S″0= S″1 | S″1 | S″2 | S″3 | S″4 | S″5 |
|---|---|---|---|---|---|---|
| $M$ (m/s) | $8.1 \cdot 10^{-8}$ | $5.6 \cdot 10^{-8}$ | $\mathbf{6.10 \cdot 10^{-8}}$ | $6.6 \cdot 10^{-8}$ | $7.0 \cdot 10^{-8}$ | $7.5 \cdot 10^{-8}$ |
| $\tau_{cd}$(N/m$^2$) | 1.235 | 1.18 | **1.2** | 1.21 | 1.22 | 1.23 |
| $\tau_{ce}$ (N/m$^2$) | 0.989 | 1.15 | **1.1** | 1.07 | 1.05 | 1.02 |
| $d$ ($\mu$ m) | 40.2 | 32 | **34** | 36.5 | 37 | 38.5 |

*Note*. S″2 (in bold) corresponds to the set of parameters with minimum quadratic error.

discharge of Scenario A. In Section P5 in Scenario A, the solid discharge is insignificant; however, in Scenario B, it increases with time as the water level decreases, to values greater than 1,000 kg/s after the first 3 days. For the 3 days after the flood, it can be seen that the water releases of 600 m$^3$/s are not enough to increase the shear stress above the critical values of erosion; thus, there is no suspended sediment transport. It is worth noting that since the Mequinensa reservoir is over 100-km long, the water released through that dam does not carry any sediment. For Scenario B, the double effect of lowering the reservoir and increasing the discharges induces solid discharges above 1,800 kg/s through Section P5, while values in normal operation do not exceed 200 kg/s. This implies that sediment is removed from the tail of the reservoir and transported to its intermediate reaches, where depths are much higher and the deposited sediments do not have such an adverse effect as in the tail itself.

Figure 14 shows the mass of sediment moving through the cross sections. It can be used to analyze the amount of sediment transported between the different areas of the reservoir in different scenarios. In Scenario A, more than approximately 50 Mkg of sediment crosses Section P1; most is deposited between Section P2 and Section P3; almost no sediment crosses Section P5. Scenario B experiences completely different sediment behavior. Here the greater volume of sediment is through Section P5, implying there is erosion in the whole reach between Section P1 and Section P5. The volume of sediment that is mobilized in Scenario B (190 Mkg through Section P1 and 370 Mkg through Section P5) is much greater than in Scenario A, implying that increasing the discharges and decreasing the water depth has the overall effect of entraining sediment between Sections P1 and P5, which is later deposited in deeper areas of the reservoir.

## 5. Discussion

The detailed description of the sedimentary processes in reservoirs is a relevant challenge for their management. The required information can only be acquired by means of complex bathymetric campaigns followed by the postprocess of great amounts of spatially distributed data. To summarize the erosion and deposition sediment processes along a longitudinal profile of a watercourse, the ASV curve presented in Figure 4 has been proven to be a practical and useful tool, since it provides the general picture of the involved processes. With such curves, it is possible to summarize in a single figure the sediment dynamics within a reach and filter oscillations inherent to field data and common in the sedimentary processes.

The results of the analysis of two different bathymetries in the Riba-roja reservoir showed that for a major flood episode, erosion and sedimentation processes took place at the reservoir tail. Previously deposited

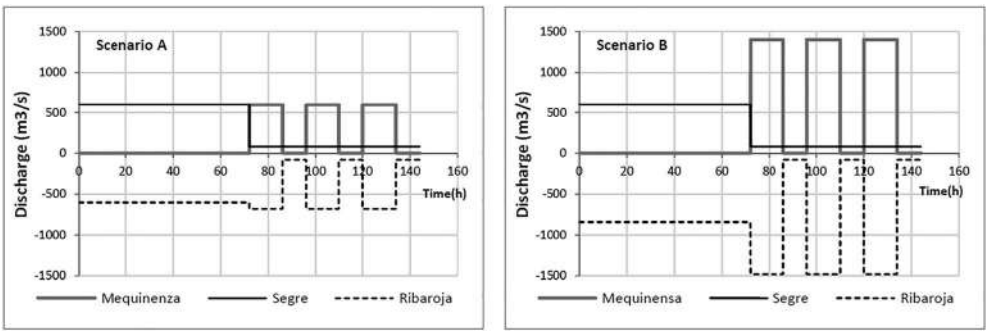


**Figure 10.** Boundary conditions of the sediment relocation example cases.

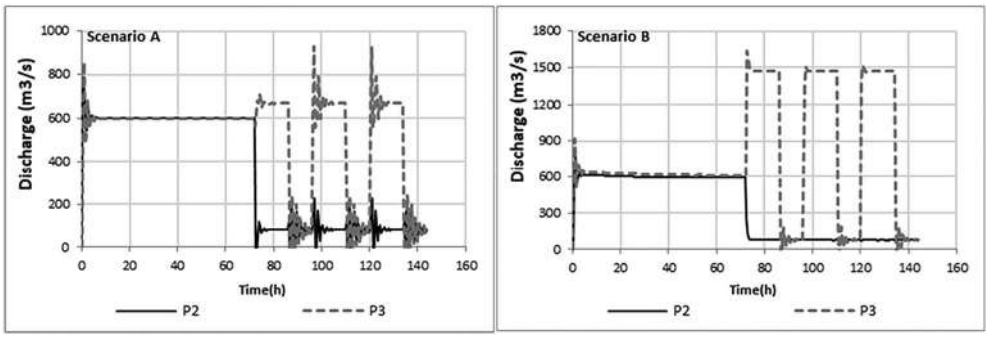


**Figure 11.** Discharge crossing control sections with normal reservoir operation (A) and with sediment relocation enhancing strategies (B).

sediment at the reservoir tail was resuspended and displaced downstream to the reservoir vase. The observed differences in the reservoir bottom elevations before and after the flood were less than a few tens of centimeters (up to 20–30 cm). Moreover, it was determined that the differences were greater in the profile along the thalweg than near the reservoir banks. Nevertheless, the total volume of the mobilized sediment, approximately 170,000 $m^3$, was significant in relation to the estimated average annual suspended sediment transport of around 370,000 Mkg (Roura Carol et al., 2008); this, once deposited, considering porosity, would be equivalent to a volume of 356,000 $m^3$.

Usually, numerical models are applied to real cases with characteristics that differ significantly from the controlled situations where the basic equations used by the models are deduced. Thus, calibration with real data is imperative to obtain quantitative results using sediment transport numerical models; a simple but well calibrated model can be more useful than one based on more complex processes and equations with more uncertain calibration.

Although the numerical models of sediment dynamics at large scales can be expected to represent average tendencies and mean values, it is not realistic to pursue an exact fit to the observed oscillations of the bed variation line in Figure 4. These oscillations can be filtered by using the ASV curve, which shows the erosion/deposition patterns along the reservoir at a glance.

To obtain the parameters that fit this curve, a process of successive approximations has been applied using a cascade of models, from simpler to more detailed ones. It was observed that an excessive 1-D simplification was not enough, since a satisfactory fitting with the curve could not be achieved. With simple 2-D models, a set of values that could reproduce the ASV curve was obtained; however, when these values were used with a much more detailed mesh, discrepancies appeared between the results and the observations. Thus, a final tuning of the parameters was performed to improve the calibration of the final model as is shown in Table 2. The information for this final tuning was obtained using the tendencies in the results of simulation S′. More explicitly, we looked among the S′ simulations (with the 2-D simplified model) for the one, referred to as S′*, that better fitted the S′0 curve. Comparing the S′* and S′1 parameters, it was observed that to adjust the curve S′* to the curve S′1, M, $d$, and $\tau_{cd}$ would have to be reduced, while $\tau_{ce}$ would have to be increased. Thus, it is reasonable to think that similar adjustments of the S″0 parameters could lead to the fitting of the numerical results with the observed ASV curve.

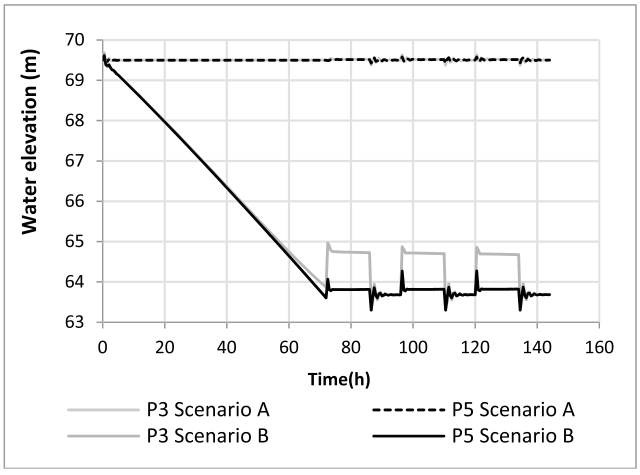


**Figure 12.** Scenario A shows the water elevation evolution with normal reservoir operation; Scenario B shows the reservoir drawdown for the sediment relocation enhancing strategies.

Once the model is calibrated, it can be used to analyze more efficient sediment relocation strategies. For example, since the Mequinensa reservoir (1,590 $hm^3$) is much larger than the Riba-roja reservoir (210 $hm^3$), the first idea for sediment relocation could be, and has been in the past, to increase discharges from the Mequinensa Dam. Nevertheless, the results of scenarios A and B conclude that for sediment relocation, the effect of partial

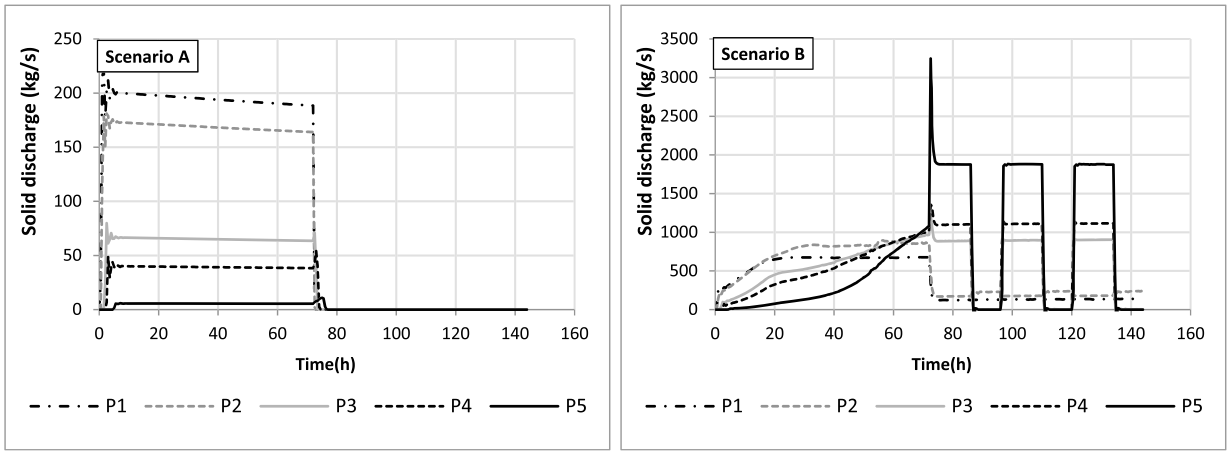


**Figure 13.** Sediment discharge crossing control sections with normal reservoir operation (Scenario A) and with sediment relocation enhancing strategies (Scenario B).

drawdowns is significantly larger than the effect of increasing discharges. This last conclusion is important from the point of view of water resources: a partial drawdown in the Riba-roja reservoir of 6 m can be conducted with a water release of approximately 80 $hm^3$ (Arbat Bofill, 2015), much less than the water releases considered in Scenario B (225 $hm^3$). This drawdown, in combination with a natural flood from the Segre River or one of its tributaries, would be highly effective since there are big deposits of sediment in the Segre immediately upstream of its confluence with the Ebro River. Since there exists no upper dams near the study area in these rivers, the arrival of floods can be easily predicted in advance and relocation strategies planned. Moreover, as the Mequinensa reservoir, upstream of Riba-roja reservoir in the Ebro River, has a much larger volume than the Riba-roja reservoir, it is possible to revert the drawdown with water from the Mequinensa with almost no effect on its water surface elevation. Generally, the Riba-roja and Mequinensa reservoirs are maintained with nearly constant levels to obtain maximum benefits from hydropower generation.

Application of the proposed methodology allows the exploration of scenarios for comparative purposes; strict validation of the approach can only be obtained through the real-life implementation of sediment management operations, duly monitored, and carefully analyzed.

Another interesting result from the application is that with normal water levels, the effect of an intermediate flood of 600 $m^3/s$ in the Segre River, in combination with the closure of the gates and power plant of the Mequinensa Dam, is primarily the resuspension of sediment in the Segre upstream of the confluence and the subsequent settlement immediately downstream of it (in Figure 14). This effect can be used to remove

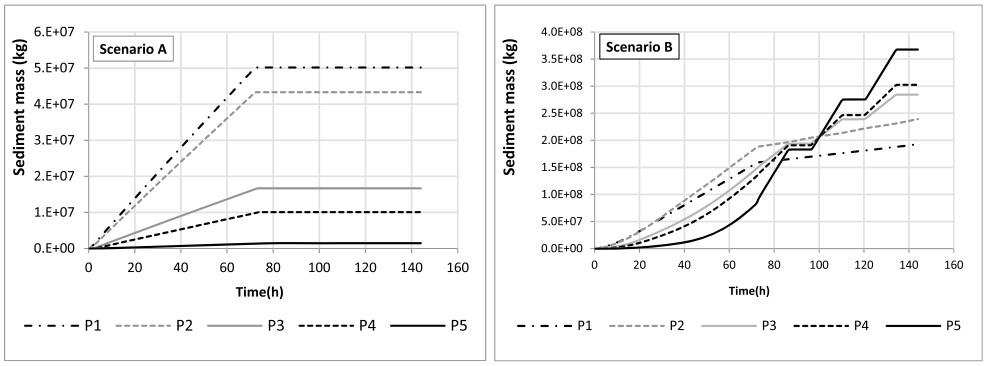


**Figure 14.** Mass of sediment crossing control sections with normal reservoir operation (Scenario A) and with sediment relocation enhancing strategies (Scenario B).

sediment deposited in that area, in front of the village of Mequinensa, which has a disused boat race stadium due to the lack of the required depth caused by sedimentation.

## 6. Conclusion

A methodology to calibrate the 2-D numerical models of sediment dynamics in a watercourse has been presented. The method uses the ASV curve and is based on a first calibration of the parameters using the Monte Carlo method and simplified models. Once the range of the involved parameters and their influence on the results is established, the final calibration is performed by fine tuning the parameters in the final detailed model. Direct calibration using the final detailed model would be extremely time consuming.

This calibration methodology, apart from saving considerable computation time, since it involves only a minimum number of simulations with the final model, provides information to understand the sedimentary processes taking place in the study area and the effect of the parameters involved in numerical simulations.

The ASV curve was used for model calibration; however, it has also proven to be a practical way to summarize the sedimentary processes along a watercourse and the results of sediment dynamics models.

The application case showed the utility of sediment transport models as a practical tool for reservoir sediment management in rivers and reservoirs; in this case, for a comparative assessment of the effect of different sediment management strategies. For the particular case of the Riba-roja reservoir in the Ebro River, it was observed that with the combination of a moderate natural flood with a limited partial reservoir drawdown, it is possible to increase the natural entrainment of the deposited sediments and relocate them to deeper areas of the reservoir.

**Acknowledgments**
The authors want to thank Confederación Hidrográfica del Ebro (CHE) and ENDESA for founding different projects which enabled the data acquisition for the present study. Hydraulic and hydrologic data for this paper can be downloaded from the SAIH Ebro website (http://www.saihebro.com). Bathymetric data can be found in the Zenoido repository (Bladé & Sanchez-Juny, 2018).

## References

Antoine, G., Besnier, A.-L., Jodeau, M., Camenen, B., & Esteves, M. (2014). Numerical modeling of suspended sediment transport during dam flushing: from reservoir dynamic to downstream propagation. In *Reservoir sedimentation—Special session on reservoir sedimentation of the 7th International Conference on Fluvial Hydraulics, River Flow 2014* (pp. 175–184). Lausanne, Switzerlan: Balkema.

Arbat Bofill, M. (2015). Distribución de temperatura y velocidad de embalses: Análisis numérico-experimental aplicado a los embalses de Sau (Ter) y Ribarroja (Ebro). TDX (Tesis Doctorals en Xarxa). Retrieved from http://www.tdx.cat/handle/10803/318591

Ariathurai, R., & Arulanandan, K. (1978). Erosion rates of cohesive soils. *Journal of the Hydraulics Division*, *104*(2), 279–283.

Avendaño, C., Sanz-Montero, M. E., & Cobo, R. (2000). State of the art of reservoir sedimentation management in Spain. In *Proceedings of the International Workshop and Symposium on Reservoir Sedimentation Management* (pp. 27–34). Toyama, Japan: Water Resources Environment Technology Center-Japan (WEC).

Bladé, E., Cea, L., & Corestein, G. (2014). Numerical modelling of river inundations. *Ingeniería Del Agua*, *18*(1), 68. https://doi.org/10.4995/ia.2014.3144

Bladé, E., Cea, L., Corestein, G., Escolano, E., Puertas, J., Vázquez-Cendón, E., et al. (2014). Iber: herramienta de simulación numérica del flujo en ríos. *Revista Internacional de Métodos Numéricos para Cálculo y Diseño en Ingeniería*, *30*(1), 1–10. https://doi.org/10.1016/j.rimni.2012.07.004

Bladé, E., & Sanchez-Juny, M. (2018). Riba-roja reservoir bathymetries [Data set]. https://doi.org/10.5281/zenodo.1483473

Blais, J. M., & Kalff, J. (1995). The influence of lake morphometry on sediment focusing. *Limnology and Oceanography*, *40*(3), 582–588. https://doi.org/10.4319/lo.1995.40.3.0582

Castillo, C., Pérez, R., & Gómez, J. A. (2014). A conceptual model of check dam hydraulics for gully control: Efficiency, optimal spacing and relation with step-pools. *Hydrology and Earth System Sciences*, *18*(5), 1705–1721. https://doi.org/10.5194/hess-18-1705-2014

Castillo, L. G., Carrillo, J. M., & Álvarez, M. A. (2015). Complementary methods for determining the sedimentation and flushing in a reservoir. *Journal of Hydraulic Engineering*, *141*(11), 05015004. https://doi.org/10.1061/(ASCE)HY.1943-7900.0001050

Cea, L., Bermúdez, M., Puertas, J., Bladé, E., Corestein, G., Escolano, E., et al. (2016). IberWQ: New simulation tool for 2D water quality modelling in rivers and shallow estuaries. *Journal of Hydroinformatics*, *18*(5), 816–830. https://doi.org/10.2166/hydro.2016.235

Cea, L., & Bladé, E. (2015). A simple and efficient unstructured finite volume scheme for solving the shallow water equations in overland flow applications. *Water Resources Research*, *51*, 5464–5486. https://doi.org/10.1002/2014WR016547

Dolz, J., Armengol, J., Roura, M., De Pourcq, K., Arbat, M., & López, P. (2009). *Estudio de la dinámica sedimentaria y batimetría de precisión del embalse de Ribarroja*. Barcelona: Flumen Institute. Universitat Politècnica de Catalunya.

Duan, J. G., & Nanda, S. K. (2006). Two-dimensional depth-averaged model simulation of suspended sediment concentration distribution in a groyne field. *Journal of Hydrology*, *327*(3–4), 426–437. https://doi.org/10.1016/j.jhydrol.2005.11.055

Einstein, H. A., & Krone, R. B. (1962). Experiments to determine modes of cohesive sediment transport in salt water. *Journal of Geophysical Research*, *67*(4), 1451–1461. https://doi.org/10.1029/JZ067i004p01451

Felix, D., Albayrak, I., Abgottspon, A., & Boes, R. M. (2016). Optimization of hydropower plants with respect to fine sediment focusing on turbine switch-offs during floods. *IOP Conference Series: Earth and Environmental Science*, *49*, 122011. https://doi.org/10.1088/1755-1315/49/12/122011

Gibson, S. A., & Boyd, P. (2014). Modeling long term alternatives for sustainable sediment management using operational sediment transport rules. In *Reservoir sedimentation—Special session on reservoir sedimentation of the 7th International Conference on Fluvial Hydraulics, River Flow 2014* (pp. 229–236). Lausanne, Switzerland: Balkema.

Guertault, L., Camenen, B., Peteuil, C., Paquier, A., & Faure, J. B. (2016). One-dimensional modeling of suspended sediment dynamics in dam reservoirs. *Journal of Hydraulic Engineering*, *142*(10), 04016033. https://doi.org/10.1061/(ASCE)HY.1943-7900.0001157

Huybrechts, N., & Villaret, C. (2010). Comparison between 2D and 3D modelling of sediment transport: Application to the dune evolution. In A. Dittrich (Ed.), *River Flow 2010* (pp. 887–893). Braunschweig, Germany, Karlsruhe: Bundesanstalt für Wasserbau.

James, W. F., & Barko, J. W. (1993). Sediment resuspension, redeposition, and focusing in a small dimictic reservoir. *Canadian Journal of Fisheries and Aquatic Sciences*, *50*(5), 1023–1028. https://doi.org/10.1139/f93-118

Kostic, S., & Parker, G. (2003). Progradational sand-mud deltas in lakes and reservoirs. Part 1. Theory and numerical modeling. *Journal of Hydraulic Research*, *41*(2), 127–140. https://doi.org/10.1080/00221680309499956

Likens, G. E., & Davis, M. B. (1975). Post-glacial history of Mirror Lake and its watershed in New Hampshire, U.S.A.: An initial report. *Verhandlungen Internationale Vereinigung Limnologie*, *19*, 982–993.

Lobera, G., Batalla, R. J., Vericat, D., López-Tarazón, J. A., & Tena, A. (2016). Sediment transport in two Mediterranean regulated rivers. *Science of the Total Environment*, *540*, 101–113. https://doi.org/10.1016/j.scitotenv.2015.08.018

López, P., Dolz, J., Arbat, M., Armengol, J., & Arbat-Bofill, M. (2012). Physical and chemical characterisation of superficial sediment of the Ribarroja Reservoir (River Ebro, NE Spain). *Limnetica*, *31*(2), 321–334.

Mahmood, K. (2005). In M. G. Anderson, & J. J. McDonnell (Eds.), *Encyclopedia of hydrological sciences*. Chichester, UK: John Wiley. https://doi.org/10.1002/0470848944

Morris, G. L., Annandale, G. W., & Hotchkiss, R. (2008). Reservoir Sedimentation. In *Sedimentation engineering processes measurements modeling and practice ASCE manuals and reports on engineering practice No 110*, (Chapter 13, pp. 579–612). Reston: ASCE.

Palau Ybars, A. (1998). Estudio limnológico del ecosistema fluvial afectado por los vaciados del embalse de Barasona. *Limnetica*, *14*, 1–15.

Partheniades, E. (1965). Erosion and deposition of cohesive soils. *Journal of the Hydraulics Division*, *91*(1), 105–139.

Prats Rodríguez, J., Morales Baquero, R., Dolz Ripollés, J., & Armenol Baquero, J. (2014). Contributions from limnology to reservoir management. *Ingeniería Del Agua*, *18*(1), 80. https://doi.org/10.4995/ia.2014.3145

Roe, P. (1986). Discrete models for the numerical analysis of time dependent. *Journal of Computational Physics*, *63*(2), 458–476. https://doi.org/10.1016/0021-9991(86)90204-4

Roura Carol, M., Armengol, J., Fernando, J., & Dolz Ripollès, J. (2008). Incidencia en los embalses de Mequinenza y Ribarroja en el transporte sólido en suspensión del río Ebro. *Ingeniería Del Agua*, *15*(4), 221. https://doi.org/10.4995/ia.2008.2936

Ruiz-Villanueva, V., Bladé, E., Sánchez-Juny, M., Marti-Cardona, B., Díez-Herrero, A., & Bodoque, J. M. (2014). Two-dimensional numerical modeling of wood transport. *Journal of Hydroinformatics*, *16*(5), 1077–1096. https://doi.org/10.2166/hydro.2014.026

Tarekegn, T. H., Toffolon, M., Righetti, M., & Siviglia, A. (2014). Modelling suspended sediment wave dynamics of reservoir flushing. In *Reservoir sedimentation—Special session on reservoir sedimentation of the 7th International Conference on Fluvial Hydraulics, River Flow 2014* (pp. 163–173). Lausanne, Switzerland: Balkema.

Van Rijn, L. C. (1987). *Mathematical modelling of morphological processes in the case of suspended sediment transport*. The Netherlands: Delft.

Vázquez-Cendón, M. E. M. E. (1999). Improved treatment of source terms in upwind schemes for the shallow water equations in channels with irregular geometry. *Journal of Computational Physics*, *148*(2), 497–526. https://doi.org/10.1006/jcph.1998.6127

Wang, Z., & Hu, C. (2009). Strategies for managing reservoir sedimentation. *International Journal of Sediment Research*, *24*(4), 369–384. https://doi.org/10.1016/S1001-6279(10)60011-X

Wen Shen, H. (1999). Flushing sediment through reservoirs. *Journal of Hydraulic Research*, *37*(6), 743–757. https://doi.org/10.1080/00221689909498509